Chemical Physics 36 (1979) 291–305

TIME EVOLUTION OF THE PULSED HF CHEMICAL LASER SYSTEM. I. KINETIC MODELING – ROTATIONAL NONEQUILIBRIUM ‡

A. BEN-SHAUL and S. FELIKS
Department of Physical Chemistry, The Hebrew University of Jerusalem, Jerusalem, Israel

and

O. KAFRI
Nuclear Research Center Negev, P.O.B. 9001 Beer-Sheva, Israel

Received 10 July 1978

A detailed model of a pulsed $F + H_2 \rightarrow HF + H$ laser is used to investigate the kinetic behaviour of the system and to provide input data for a thermodynamic analysis of its time evolution. The rate equations for all relevant vib-rotational level populations and photon densities are solved for various initial conditions without using the rotational equilibrium assumption. The results of the kinetic model are in good agreement with the experimental results of Berry in which high inert gas pressure was used to enhance rotational relaxation. The effects of specific kinetic processes on the time evolution of the molecular populations and the laser output are evaluated by varying the inert gas pressure and by "switching on and off" the influence of various kinetic factors. The laser efficiency ranges between ≈ 1 to 2 photons per molecule. The major rate process enhancing the efficiency is rotational relaxation. The reduction in laser efficiency due to vibrational relaxation is ≈ 20%.

1. Introduction

The time evolution of a pulsed chemical laser system is determined by a complex interplay between a multitude of chemical, radiative and collisional energy transfer processes. At the microscopic level the evolution of the system is described by the rate (master) equations governing the time rate of change of the level populations and photon densities in the laser cavity. The major practical limitation on the predictive value of modeling studies based on the rate equation approach stems from the lack of complete kinetic information for all the relevant detailed rate processes. However, the rapid accumulation of reliable experimental and theoretical data on many state-to-state processes occurring in chemical laser systems gradually reduces this difficulty [1].

A complementary, macroscopic, description of the nonequilibrium laser system is provided by the time evolution of its various thermodynamic functions [2]. Chemical lasers are particularly suited and interesting for thermodynamic analyses because the coherent laser radiation which carries (ideally) no entropy is equivalent to thermodynamic work. Thus, chemical lasers (in analogy to electrochemical cells) can be treated as heat engines. In the thermodynamic approach the very detailed information provided by the solutions of the rate equations is condensed into a few macroscopically significant functions such as the entropy and energy of the system. These quantities provide additional insights into the mechanisms of energy storage, conversion and dissipation in the nonequilibrium laser system.

In this study which will be presented in two consecutive papers we present a combined kinetic–thermodynamic analysis of a typical chemical laser. We have chosen one of the best known systems, namely the HF laser based on the pumping reaction $F + H_2 \rightarrow HF + H$. This paper, hereafter I, includes the kinetic model and the microscopic description. The thermodynamic description is provided in the following paper [2], hereafter II.

In constructing the kinetic model we attempted to simulate the experimental conditions chosen by Berry

---

‡ Work supported by the Israel Academy of Sciences, The Commission for Basic Research.

[3,4] in his comprehensive study of the $F + H_2$ system (and its isotopic variants with HD, D_2). In Berry's experiments a large excess of Ar was added to the lasing mixture to enhance rotational relaxation. Nevertheless, in our kinetic model the rotational equilibrium assumption, which could greatly simplify the calculations [5,6], is not employed. This was done for two reasons. First, to allow for a systematic evaluation of rotational nonequilibrium effects by extending the calculations to low inert gas pressures. Second, to test if indeed the large excess of buffer gas could ensure complete rotational equilibrium throughout the lasing process, especially at high rotational levels the relaxation of which is known to be relatively slow [7–13]. Among the experimental indications for rotational nonequilibrium in chemical lasers are multiline operation, R-branch transitions and pure rotational transitions ‡. Our rate equations involve all the relevant vib-rotational levels of the lasing molecules as well as all the significant radiative transitions. A sample of thereotical work in which the effects of rotational nonequilibrium were studied is provided in refs. [15–20].

In addition to investigating the general kinetic behaviour of the laser system we intend to test here the capability of modeling studies to simulate experimental results. The choice of the relatively simple and well studied flash initiated HF system [3] is in line with this objective. Yet, this system as well involves several unknown kinetic factors. For example, the relaxation rates of vibrationally excited HF molecules due to different collision partners, the rates of secondary chemical reactions, the exact time profile and quantum efficiency of the flash pulse and the extents of useful output coupling and dissipative losses. Since we attempted to avoid extensive optimizations not all the experimental results could be exactly reproduced. However, in many respects the agreement with experiment is good.

2. The kinetic model

The time evolution of the pulsed HF laser system will be described in the rate equation approximation [5,6,15–20]. The rate processes included in the modeling are listed in table 1. Since we do not employ the rotational equilibrium assumption the rate equations involve all the significant vib-rotatinal populations $N_{vJ} = [\mathrm{HF}(v,J)]$ and photon densities ϕ_{vJ} corresponding to P-branch transitions $v,J-1 \rightarrow v-1,J$. $\phi_{vJ} = \rho_{vJ}/h\nu_{vJ}$, where ρ_{vJ} is the energy density at the transition frequency $\nu_{vJ} = (E_{v,J-1} - E_{v-1,J})/h$. Since P-branch transitions are considerably stronger than R-branch transitions originating in the same level, except possibly under very peculiar rotational nonequilibrium conditions [14,18] we do not incorporate R-branch transitions in the modeling.

Table 1
The kinetic scheme

Initiation

$$CF_3I \xrightarrow[\text{flash}]{h\nu} CF_2I + F \tag{R-1}$$

Pumping

$$F + H_2 \rightleftharpoons HF(v,J) + H \tag{R-2}$$

Secondary reaction

$$F + CF_3I \rightarrow CF_3 + FI \tag{R-3}$$

Stimulated and spontaneous radiation. (P-branch)

$$HF(v,J-1) \overset{h\nu_{vJ}}{\rightleftharpoons} HF(v-1,J) + h\nu_{vJ} \tag{R-4}$$

R–R, T transfer

$$HF(v,J) + M \rightleftharpoons HF(v,J') + M \tag{R-5}$$

V–V transfer

$$HF(v,J) + HF(v',J') \rightleftharpoons HF(v \pm 1,J) + HF(v' \mp 1,J') \tag{R-6}$$

$$HF(v,J) + H_2(0) \rightleftharpoons HF(v-1,J) + H_2(1) \tag{R-7}$$

V–R,T transfer

$$HF(v,J) + M_i \rightleftharpoons HF(v',J) + M_i \tag{R-7+i}$$

$$M_1,\ldots,M_7 = F, H, HF, H_2, Ar, CF_3I, CF_3 \qquad i = 1-7$$

Assuming that the radiative and chemical processes are uniform along the laser axis, the population and photon equations are of the form

$$\mathrm{d}N_{vJ}/\mathrm{d}t = S(v,J) - R(v,J) - D(v,J), \tag{1}$$

$$\mathrm{d}\phi_{vJ}/\mathrm{d}t = G(v,J) - L(v,J). \tag{2}$$

Here $S(v,J)$ symbolizes the chemical pumping term, $R(v,J)$ and $D(v,J)$ represent the net depletion of v,J due to radiative and collisional energy transfer processes, respectively. $G(v,J)$ stands for the gain of photons with

---

‡ For a sample of experimental observations of rotational nonequilibrium effects, see e.g. refs. [14].

frequency ν_{vJ} and $L(v,J)$ accounts for the useful and useless output coupling.

The levels considered in the modeling are those which can be populated by the pumping reaction or other rate processes. The following levels were taken into account: All the rotational levels between $J = 0$ and 19 in the $v = 0$ manifold, $J = 0 - 16$ in $v = 1$, $J = 0 - 16$ in $v = 2$ and $J = 0 - 8$ in $v = 3$. The equations for higher rotational levels as well as the $v \geqslant 4$ levels have been omitted after solving an extended set of equations and verifying that their populations are negligible throughout the lasing. Based on similar tests the P-branch transitions considered in the modeling are $P_{1\to 0}(1-16)$, $P_{2\to 1}(1-16)$ and $P_{3\to 2}(1-8)$, where $P_{v\to v-1}(J)$ represents $v,J-1 \to v-1,J$. Hence, we have 67 population equations and 40 photon equations. These equations are solved simultaneously with the equations for the nonlasing species and the translational temperature.

Writing up the explicit form of the various contributions to (1) and (2) is a rather tedious but straightforward procedure. Therefore in the following descripttion we shall consider only few terms and focus the discussion on the choice of some of the rate constants. We shall use k_j and k_{-j} for the forward and reverse rate contants of reaction (R-j) in table 1. Further details and numerical values are provided in the appendix.

2.1. Initiation

The chemical species present in the cavity at $t = 0$ are [3] CF_3I, H_2 and Ar. In all calculations we have taken $[CF_3I]_0 = [H_2]_0 = 5.15 \times 10^{-8}$ mole/cm^3 corresponding to $P = 1$ torr at the initial temperature, $T = 300$ K. The Ar pressure which determines the rate of rotational relaxation and affects the linewidth and the temperature rise was taken as a variable. In the "standard run" $P_{Ar} = 50$ torr, in accordance with the experimental run with which our results will be compared.

The F atoms required for the pumping reaction, (R-2), are generated by flashphotolysis of CF_3I molecules, (R-1). The secondary reaction, (R-3), is reported [21] to be faster than the pumping reaction and thus consumes more F atoms. The rate equations for the various chemical species are

$$d[CF_3I]/dt = -\psi(t)[CF_3I] - k_3[F][CF_3I], \qquad (3)$$

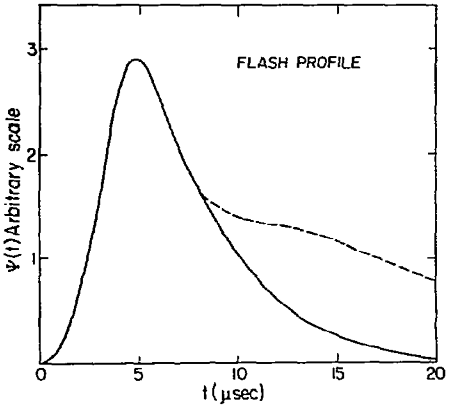

Fig. 1. The experimental flash profile (dashed line) and the fitted (full line) flash profile used in the model. The tail of the experimental profile was treated as a noise since otherwise lasing would last long beyond the experimental pulse duration. The origin of the time scale of the figure is shifted by 1 μs with respect to the time scale of ref. [3].

$$d[F]/dt = \psi(t)[CF_3I] - k_3[F][CF_3I] - k_2[F][H_2] + \sum_{vJ} k_{-2}(v,J)[H]N_{vJ}, \qquad (4)$$

$$-d[H_2]/dt = d[H]/dt = d[HF]/dt = k_2[F][H_2] - \sum_{vJ} k_{-2}(v,J)[H]N_{vJ}, \qquad (5)$$

where $\psi(t)$ is proportional to the flash profile and $k_2 = \Sigma k_2(v,J)$ is the overall pumping rate constant. The reverse process in the exothermic secondary reaction (R-3) is neglected so that $d[CF_3]/dt = d[FI]/dt$ are given by the second term in (3).

The time dependence of $\psi(t)$ was fitted to the experimental flash profile except for truncating the long tail which extends far beyond the laser pulse, fig. 1. The numerical constants entering $\psi(t)$, (see appendic), were determined by the requirement [3] that the total loss of $[CF_3I]$ is 23%. The fraction of F atoms yielding finally HF molecules is a function of k_2/k_3. In the standard run we have used $k_3/k_2 = 4.5$ which lies within the (large) experimental error bounds associated with k_3 and provides good agreement with the experimental results. (The agreement could be somewhat improved

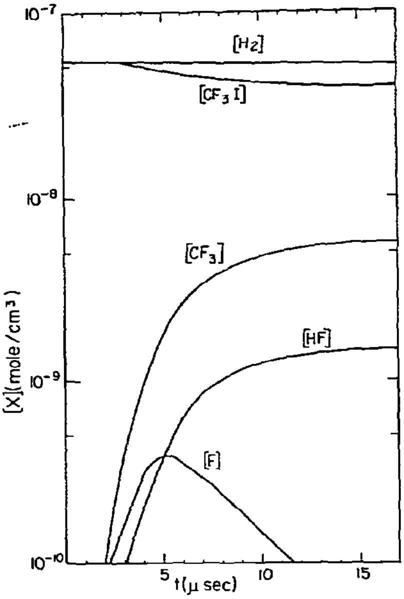

Fig. 2. Chemical species concentration as function of time.

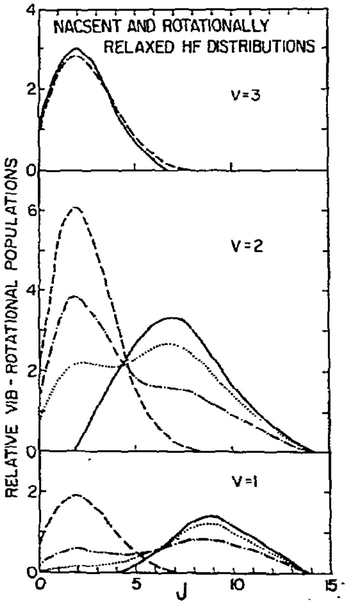

Fig. 3. The vib-rotational distribution of the nascent products in the pumping reaction (——). The two partly relaxed distributions denoted by dotted (...) and dashed-dotted (–.–.–) lines illustrate the combined effect of pumping and rotational relaxation (according to eq. (11)). These, pre-threshold, distributions represent the relative populations in the standard run (P_{Ar} = 50 torr) at t = 0.04 and 0.1 μs, respectively. Also shown, are the Boltzmann distributions (– –) in the various vibrational levels.

by choosing a smaller ratio, see below.) The time dependence of the concentrations of the various chemical species is shown in fig. 2.

2.2. *Pumping*

The pumping term in (1) is

$$S(v,J) = k_2(v,J)[\mathrm{F}]\,[\mathrm{H}_2] - k_{-2}(v,J)[\mathrm{H}]N_{vJ}. \qquad (6)$$

Here, $k_2(v,J) = k_2P(v,J) = k_2P(v)P(J|v)$, where k_2 and $P(v,J)$ are the total rate constant and the nascent product vib-rotational distribution of the pumping reaction. $P(v) = \Sigma_J P(v,J)$ and $P(J|v)$ are, respectively, the nascent vibrational and rotational distribution functions. The value of k_2, like most other total rate constants, was taken from the recommended list of ref. [22]. $P(v)$ is based on chemical laser [3] and IR chemiluminescence measurement [23]. The chemiluminescence measurements [23] provide also $P(J|v)$. $P(v,J)$ is shown in fig. 3.

In order to test the rotational equilibrium assumption some of the calculations were carried out with hypothetical rate constants of the form $k_2(v,J) = k_2(v)P_{\mathrm{B}}(J|v) = k_2P(v)P_{\mathrm{B}}(J|v)$, where $P_{\mathrm{B}}(J|v)$ is the normalized Boltzmann rotational distribution in level v; $P(v)$ is the nascent vibrational distribution. These rate constants ensure that the pumping reaction populates the rotational levels in a Boltzmann fashion. (It should be noted however that $P(J|v)$ implies $\langle f_{\mathrm{R}}\rangle = 0.08$ while $P_{\mathrm{B}}(J|v)$ leads to $\langle f_{\mathrm{R}}\rangle \approx 0.02$. f_{R} is the fraction of the reaction exoergicity appearing as product's rotational energy.) To ensure that the Boltzmann shape is preserved throughout the lasing it is necessary to assume instantaneous rotational relaxation (section 3).

2.3. *Radiation*

The radiation terms in (1) and (2) are

$$G(v,J) = c\,\sigma_{vJ}\,\Delta N_{vJ}\,\phi_{vJ} - \alpha A_{vJ}, \qquad (7)$$

$$R(v,J) = -G(v,J) + G(v-1,J+1), \qquad (8)$$

$$L(v,J) = \phi_{vJ}/\tau_{\mathrm{p}} = c\,\sigma_{vJ}\,\Delta N^{\mathrm{th}}_{vJ}\,\phi_{vJ}, \qquad (9)$$

where $\Delta N_{vJ} = N_{v,J-1} - [(2J-1)/(2J+1)]N_{v-1,J}$ is the population inversion, $\Delta N_{vJ}^{\mathrm{th}}$ is the Einstein coefficient for spontaneous emission and α is the effective fraction of photons emitted spontaneously along the laser axis. σ_{vJ} is the cross section for stimulated emission

$$\sigma_{vJ} = g(\nu_{vJ})\, B_{vJ}\, h\nu_{vJ}/c, \tag{10}$$

where B_{vJ} is the Einstein coefficient for stimulated emission ‡ and $g(\nu_{vJ})$ is the lineshape function. $g(\nu_{vJ})$ was taken as a convolution of the Doppler and Lorentz (pressure) profiles, i.e. $g(\nu)$ is the Voigt function [3]. It is assumed that lasing occurs at line center and drains the entire profile homogeneously. The spontaneous emission term in (7) is necessary to ignite the amplification process but can be neglected after threshold. Thus, we ignored its effect on the populations (by omitting the second term of (7) from the G terms in (6)). In all calculations we have used $\alpha = 10^{-4}$. Also, since only relative pulse energies are reported in ref. [3] it was assumed that (9) represents only useful output coupling, thereby disregarding the dissipative losses of radiation. The photon lifetime was estimated as $\tau_p = 10^{-7}$ s, based on the resonator geometry reported in ref. [3].

2.4. Rotational relaxation

The R–T relaxation model employed in the modeling is [7]

$$k(v,J \to v,J') = k(J \to j'|v) = fA(T)$$

$$\times \exp[-C(E_{v,J} - E_{v,J'})], \quad J > J' \tag{11}$$

with $|\Delta J| = 1,2,3$. $k(J' \to J|v)$ for $J' < J$ are calculated by detailed balancing. The numerical values of C, which measures the decrease of $k(J \to J'|v)$ with J, ($E_{vJ} - E_{v,J'} \approx 2BJ, J' = J-1$), and A, which determines its absolute magnitude are given in the appendix. f is a scaling factor which can be regarded as a measure for the efficiency of R–T transfer. In the standard run $f = 1$. It was assumed that (11) is independent of the collision partner. Alternatively, (11) is the average rate constant for all species. Some rotational relaxation patterns for pre-threshold times, i.e. when the pumping and R–T processes are active but lasing have not yet started are shown in fig. 3.

A slightly different R–T relaxation model is [8,12, 13]

$$k(J \to J'|v) = f\bar{A}(T)\,(2J'+1)$$

$$\times \exp[-\bar{C}(E_{vJ} - E_{vJ'})], \quad J > J'. \tag{12}$$

This expression, being proportional to the final state degeneracy, seems physically sounder as it leads, via detailed balancing, to a reverse rate constant with the same property. In a previous study [17] we have used (12) as the R–T model after fitting it (with good agreement) to the arrested relaxation chemiluminescence measurements [22]. Since meanwhile the constant C in (11) was measured more directly [10,11], we shall use (11). However, as can be seen from fig. 4 the two models yield essentially indistinguishable results.

2.5. Vibrational relaxation

All the V–V and V–T rate constants for HF collisions with F,H,H_2 and HF are based on the recommended list of ref. [22]. Of course, some of these rate constants derive from approximate theoretical models rather than experimental results and thus involve unestimated uncertainties. Also, since the recommended values refer to rotationally averaged rate constants, the J dependency of the various $k(v,J \to v',J')$ is unknown. Although it is known that in certain processes, e.g. HF + HF collisions, V–R transfer can be more effective than V–T transfer [1] and thus $|J' - J|$ may be large, we assumed that all collisions proceed with $J' = J$. This approximation is based on the results of previous studies [17,18] in which the effects of V–R transfer were examined in detail. It was found that any irregularities in the rotational distributions which might be caused by V–R transfer are rapidly washed out by the much faster R–T processes.

The V–T rates corresponding to CF_3I and Ar are small but are included in the modeling. The values attributed to the rate constant for CF_3 radicals are arbitrary and should be regarded as lumping together the V–T deactivation rates due to all unknown chemical species in the system as well as accounting for uncertainties in the rate constants taken from ref. [22]. The values cited in the appendix were used in the standard run.

---

‡ Numerical values for Einstein's coefficients from ref. [24] (see also ref. [5]). Transition frequencies from ref. [25].

2.6. Other variables

The equation for the translational temperature which appears as a parameter in the collisional and radiative (via the linewidth) rate coefficients is

$$\mathrm{d}T/\mathrm{d}t = \frac{1}{C_v}\left[\sum_i E_i^0\, \mathrm{d}[\mathrm{M}_i]/\mathrm{d}t + \sum_{vJ} E_{vJ}\, \mathrm{d}N_{vJ}/\mathrm{d}t + \sum_{vJ} h\nu_{vJ} G(v,J)\right], \qquad (13)$$

where the first sum extends over all chemical species, including HF. E_i^0 is the standard energy of species i measured on the energy scale of the free atoms. E_{vJ} is the energy of HF(v,J) measured from the ground level. The last term represents the rate of change of the radiation energy. C_v is the heat capacity at constant volume per unit volume. The initial temperature is $T = 300$ K.

The flash light and secondary reactions generate various chemical species in the lasing mixture [3], e.g. $\mathrm{CF_2}$, $\mathrm{CF_3H}$ and $\mathrm{I^*}$. We do not include them in the modeling, although they might be influential, due to the lack of accurate kinetic data.

2.7. Numerical method

The rate equations were integrated using Brumer's version [26] of Gear's hybrid [27] (see also ref. 18) (predictor–corrector) method.

3. Results and discussion

In this section we present and analyze the results of two, partly overlapping sets of computer experiments. The first set examines the effects of rotational equilibrium and nonequilibrium. This was achieved by varying the Ar pressure, by switching off the R–T processes and by enhancing their effects. In addition to rotational relaxation the Ar pressure affects, though to a lesser extent, the linewidths and the temperature rise. Through the second series of results we intend to evaluate the specific effects of various kinetic processes on the laser performance. The standard run which attempts to simulate the experimental results [3] serves as a reference in both sets of computer experiments. Thus, except for the specific variations characterizing a given run, all other factors remain as in the standard run. The re-

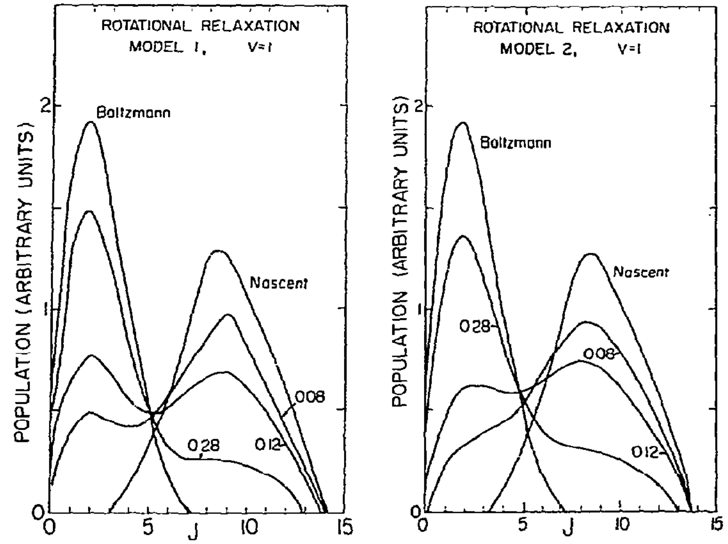

Fig. 4. Comparison of the two rotational relaxation models: Model 1 corresponds to eq. (11) and model 2 to eq. (12). Shown are the nascent, Boltzmann and intermediate rotational distributions in $v = 1$. The various curves describe pure rotational relaxation patterns, i.e. without the interference of pumping and other kinetic processes. The numbers indicate the time in microseconds. The inert gas pressure is 50 torr. The figure indicates that by an appropriate choice of the constants in (11) and (12) the two models are essentially identical.

sults of the kinetic analysis will serve as input data for the time-dependent thermodynamic analysis presented in the subsequent paper. The choice of a wide spectrum of kinetic coupling schemes will enable us to provide a comprehensive kinetic–thermodynamic picture of the chemical laser system.

For convenience, the various runs will be labelled and numbered as follows: (1) "Standard" ($P_{\mathrm{Ar}} = 50$ torr), (2) "$P_{\mathrm{Ar}} = 25$ torr"; (3) "$P_{\mathrm{Ar}} = 5$ torr", (4) "$P_{\mathrm{Ar}} = 0$", (5) "Boltzmann". Here the rotational distribution of the HF molecules is forced to be Boltzmann before, during and after the lasing. This condition was reached by replacing the nascent product distribution $P(J|v) = k_2(v,J)/k_2(v)$, by the Boltzmann distribution $P_{\mathrm{B}}(J|v) = (2J+1)\exp[-E_J(v)/kT]/q_{\mathrm{rot}}$, cf. fig. 4. In addition, the rate of R–T transfer was artificially enhanced by using $f = 2.5$ in (11). This will prevent "hole burning effects" in the rotational distributions due to radiative, pumping and relaxation processes, (6) "No R–T". This is the opposite extreme of the previous run, i.e. $f = 0$ in (11). (7) "No relaxation". Here all V–V, V–T and R–T processes have been switched off. (8) "No V–T". (9) "No V–V". (10) "No V–V and V–T". (11) "No V–T CF_3". (Recall that V–T by CF_3 is supposed to incorporate uncertainties in vibrational relaxation processes).

Runs 1–7 and 5–11 comprise the first and second sets of results, respectively. Of course, some runs will be discussed in detail while others only briefly. The discussion will be organized in three parts. First, comparison with experiment. Second, systematic analysis of R–T effects. Third, test of V–V and V–T effects.

3.1. Comparison with experiment

The results of the kinetic model will be compared with the results of Berry's free running experiment [3], with the initial pressures $CF_3I : H_2 : Ar = 1 : 1 : 50$ torr. The experimental data available for comparison are the threshold times, the shapes and the relative intensities of the various P-branch pulses. This information includes the relative intensities of the three active vibrational bands, $v = 3 \to 2$, $v = 2 \to 1$ and $v = 1 \to 0$.

The first two columns of fig. 5 compare the experimental pulse patterns [3,4] and the corresponding patterns of the standard run. Taking into account the high complexity of the system the agreement between the experimental and computed results is, in our opinion, satisfactory. This is reflected for instance by the very similar threshold times and relative intensities (spectral distributions) of most of the individual lines.

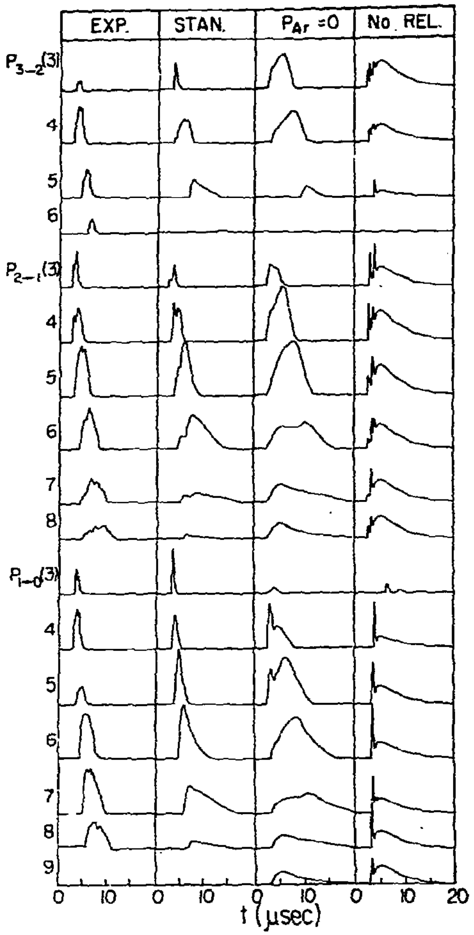

Fig. 5. Pulse patterns of the HF laser output. Shown are the experimental results (adapted from ref. [4]), and the results of the "standard" (no. 1), "$P_{\mathrm{Ar}} = 0$" (4), and "no relaxation" (7) runs. (The experimental time scale is shifted by ≈ 1 μs with respect to the results of ref. [4], see fig. 1).

The main points of variance between the experimental and computed outputs are associated with the late stages of the pulse. Namely, the longer tails of a few computed pulse patterns, the higher intensities of some high J lines in the experimental output (e.g., $P_{2\to1}(8)$, $P_{1\to0}(8)$ and $P_{1\to0}(9)$) and the later threshold times of the computed $P_{3\to2}(5,6)$ lines. Another point of departure is a difference of about 20% between the ratios of integrated intensities in bands $v = 2 \rightarrow 1$ and $1 \rightarrow 0$. While the experimental values of the relative integrated band intensities are $I_{1\rightarrow 0} : I_{2\rightarrow 1} : I_{3\rightarrow 2} = 1 : 0.79 : 0.23$ the corresponding values in the standard runs are 1 : 1.01 : 0.29 (see table 2). Hence $(I_{1\rightarrow 0}/I_{2\rightarrow 1})_{\mathrm{exp}} \approx 1.2$ $(I_{1\rightarrow 0}/I_{2\rightarrow 1})_{\mathrm{st}}$. Note that the agreement between the experimental and computed values of $I_{3\rightarrow 2}/I_{2\rightarrow 1}$ is very good.

In a system governed by so many kinetic processes (some of which are uncertain, some unknown) such as the HF laser, the variance between experimental and theoretical findings may be attributed to many factors. We shall point out some of the possible factors and then try to evaluate the more important ones. (To this end many computer experiments, besides the eleven counted above, were carried out). Among the possible reasons are: (i) Mischoice of the output coupling factor, τ_p, or the rate constant of (R-3). (ii) Inaccurate representation of the flash profile. (iii) Inaccurate description of the rotational relaxation mechanism. (iv) Unknown, or underestimated, vibrational activation and deactivation processes.

It can be shown that at complete rotational equilibrium (a condition very nearly satisfied in the standard run, see below), the range of lasing transitions and the ratios $I_{v+1\rightarrow v}/I_{v\rightarrow v-1}$ increase (slowly) with τ_p and the absolute number of lasing molecules [19]. In our model the overall production of HF molecules is an increasing function of k_2/k_3 (see appendix). However, increasing τ_p (within the uncertainty region estimated from the resonator geometry [3]) and k_2/k_3 (up to the lowest error bound on k_3, see appendix) have led only to a minor improvement in the agreement between the experimental and computed results. A similar conclusion was reached with respect to variations of the flash profile. Undoubtedly, the laser output pattern is very sensitive to the details of rotational relaxation. Namely, the functional form of the model employed, the magnitudes of constants appearing in the model (e.g., A and C in eq. (11)) and their dependence on the collision partner. Under nearly complete rotational equilibrium conditions, high J lines (such as $P_{3\rightarrow 2}(5{,}6)$ and $P_{1\rightarrow 0}(9)$) start the lasing after most of the nascent vibrational populations were drained through lower J lines, cf. fig. 5. This is due to the J shifting mechanism [3–6, 15–20] which governs the lasing at rotational equilibrium. Since the upper and lower level populations of high J lines as well as their rotational relaxation rates are small, the corresponding gain coefficients and threshold times are sensitive to variations in the rates of R–T, pumping, radiative cascades and V–T processes which populate and depopulate these levels. We found, for example, that the threshold times of $P_{3\rightarrow 2}(5{,}6)$ are somewhat shorter in the $P_{\mathrm{Ar}} = 25$ torr run than in the standard run and the intensity of $P_{1\rightarrow 0}(9)$ is higher. However, on further decrease of the R–T rate $P_{3\rightarrow 2}(6)$ vanished (fig. 5, $P_{\mathrm{Ar}} = 0$). This is because at low R–T rates the gain on this line, which is determined primarily by the nascent distribution, is negative, cf. fig. 3. In conclusion of this point we can say that the differences between the experimental and computed patterns of a few lines reflect only minor inaccuracies of the kinetic model.

The deviation of the theoretical $I_{2\rightarrow 1}/I_{1\rightarrow 0}$ value from the experimental one can be attributed to the use of two small V–T rates in the kinetic code or to unknown effects of collisions with free radicals or excited iodine atoms. Indeed, by artificially increasing the V–T deactivation of $v = 2$ and 3, the computed value of $I_{2\rightarrow 1}/I_{1\rightarrow 0}$ as well as the pulse durations, approach closer to the experimental results. However, unambiguous resolution of the differences will not be possible until more accurate kinetic data will become available. The arbitrary values assigned to the rate constant of (R-14) (table 1) represent a compromise between the lack of reliable kinetic data on the one hand and the experimental laser results on the other hand.

3.2. Rotational nonequilibrium

A systematic survey of rotational relaxation effects on the molecular level populations and the output of the HF laser is provided by runs 1–7. Since these effects have been discussed extensively elsewhere [15–20] we shall confine ourselves here in briefly describing the lasing mechanism in the two limiting cases of very fast and very slow rotational relaxation. All other cases such as the $P_{\mathrm{Ar}} = 25{,}5$ and 0 torr display intermediate behaviour. The results presented in the following will provide the kinetic background necessary for the thermodynamic analysis of the subsequent paper.

In the limit of instantaneous rotational relaxation, as idealized by the "Boltzmann" run and very nearly realized by the "standard" run, the lasing is governed by a *cooperative* or *homogeneous* mechanism. Lasing starts on the highest gain line, as determined by $P(v,J) = r_i(v)P_B(J|v)$, where $P_i(v)$ and $P_B(J|v)$ are the nascent vibrational distribution and the Boltzmann rotational distribution, respectively [4–6]. (In our case, like in the experiment [3], lasing starts on $P_{2\to 1}(3)$.) The attainment of threshold is accompanied by a sharp decrease in $P(v)/P(v-1)$, where $v \to v-1$ is the first lasing band. ($v = 2$ in our case). However, owing to the very fast R–T transfer, no holes are burnt in the rotational distributions; hence the term *homogeneous lasing mechanism*. Also, the fast R–T transfer suppresses the possibility of lasing on other lines besides the one with the highest gain. The J number of the highest gain transition is shifted upwards as $P(v)/P(v-1)$ decreases [3–6, 15–20]. Hence, in a given band the lasing which takes place on (nearly) a single at any moment is gradually shifted in time towards higher J values. Since threshold is reached nearly simultaneously on all bands, fig. 5, radiative cascades lead to some oscillations in the laser output. The single line operation and the J shifting are clearly seen in the experimental and standard output patterns shown in fig. 5. Fig. 6a illustrates the absence of hole burning effects. The abrupt changes in the relative vibrational populations following the attainment of the lasing threshold and the moderate changes afterwards are shown in fig. 7a. Inspection of figs. 5, 6a and 7a proves that most of the laser energy is extracted from partially inverted vibrational populations. More precisely, from fig. 6a and fig. 8 which show the total laser output as a function of time, we see that more than 90% of the laser energy is obtained at $t > 5$ μs where $P(v)/P(v-1)$ is typically ≈ 1/3. This highly efficient conversion of internal energy into laser light from partially inverted populations is a direct consequence of the cooperative lasing mechanism resulting from the strong rotational coupling. Namely, whenever the gain of a given J line falls below threshold, fast R–T transfer enables the system to continue lasing on the next higher J. Eventually lasing terminates because the pumping rate fails to overcome the losses by vibra-

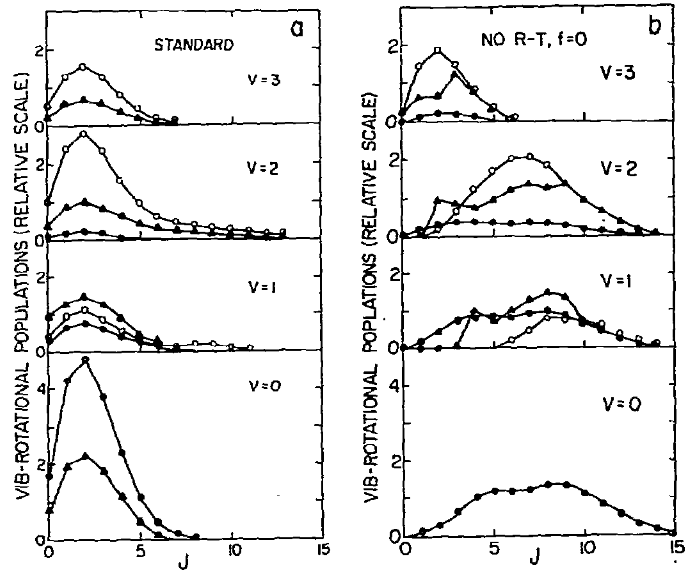

Fig. 6. Relative vib-rotational distribution shortly before threshold (○), shortly after threshold (▲) and at the end of the laser pulse (●). (a) "standard" run. The pre-threshold distributions (t = 1.96 μs), is nearly but not completely Boltzmann. The high J levels in v = 1 and 2 are not completely relaxed due to the strong pumping and the relatively low rotational relaxation of these levels. The post threshold distributions (t = 3.3 μs and 20 μs) indicate that the radiation does not burn holes in the rotational profiles. (b) No R–T, (f = 0). The pre-threshold distribution (t = 1.3 μs) is essentially identical to the nascent distribution (except for minor V–T effects). Hole burning effects are observed in the post-threshold distribution (▲, t = 3.0 μs). The final distribution (●, t = 18 μs) is a reflection of the nascent distribution.

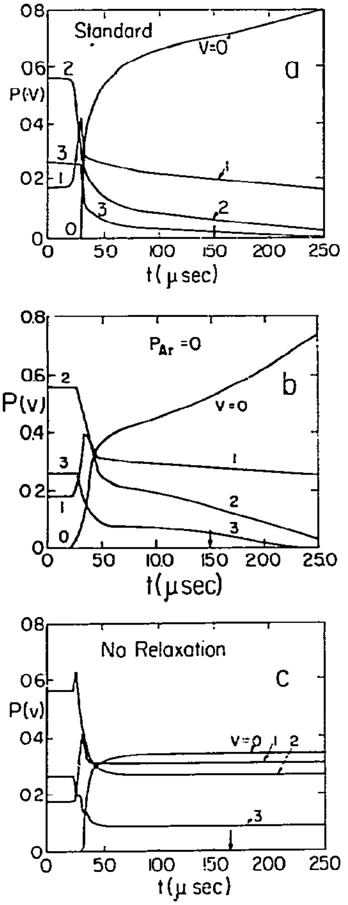

Fig. 7. The vibrational level distribution as a function of time for the "standard" (a), "$P_{Ar} = 0$" (b), and "no relaxation" (c), runs. Arrows indicate the termination of the laser pulse. The large difference between the final values of $P(v)/P(v-1)$ in (7a) and (7c) explains the very different laser efficiencies. (b) which displays intermediate behaviour shows that vibrational relaxation is negligible before threshold and gradually increases towards the end of the pulse.

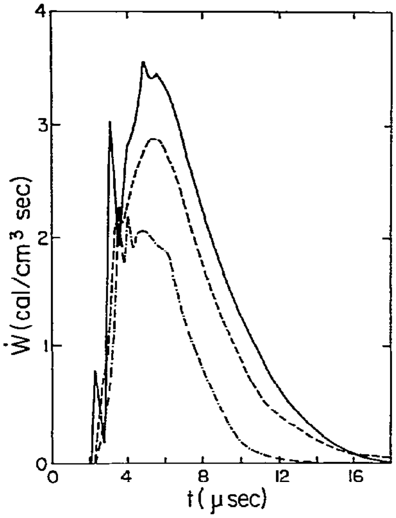

Fig. 8. Total laser output powers as function of time for the "standard", (——), "$P_{Ar} = 0$", (– – –), and "no R–T", (– . –), runs. $\dot{W}$ is the time rate of change of the laser output energy per unit volume of the laser cavity.

tional relaxation. In the absence of vibrational relaxation (as in run 10), lasing terminates because the absolute number of molecules produced by the pumping reaction does not suffice to overcome the threshold inversion [19].

In the opposite extreme, i.e. in the absence of rotational relaxation, the lasing mechanism is *individual* or *inhomogeneous* [17–19]. Here, the vib-rotational populations are affected only by radiative processes and (to a lesser extent) by vibrational relaxation. Different rotational transitions in a given band reach threshold, lase and decay independently from one another. The "$P_{Ar} = 0$" and, more drastically, the "no-relaxation" output patterns shown in fig. 5 clearly illustrate this behaviour. The spike structure in the threshold region of the last output pattern results from threshold oscillations superimposed by radiative cascades. The independent lasing mechanism leads to hole burning effects in the (nascent) rotational distributions, as shown in fig. 6b for the "no R–T" run. In this case lasing in a given $P_{v\to v-1}(J)$ line terminates when the net depletion rate of the corresponding population inversion, $N(v,J-1) - [(2J-1)/(2J+1)]N(v-1,J)$, exceeds the pumping rate. If both rotational and vibrational relaxation are absent exchanges of population can take place only within groups of vib-rotational levels connected by consecutive P-branch transitions [19], i.e. levels $v,J-1; v-1,J; v-2,J+1, \ldots$. In this case, the spectral distribution of the laser output is a direct reflection of the nascent vib-rotational distribution. This feature is displayed by the spectral distribution obtained in the "no R–T" run shown in fig. 9. (The V–T effects included in this run represent only a minor perturbation.) The peak in $v = 3 \to 2$ corresponds to

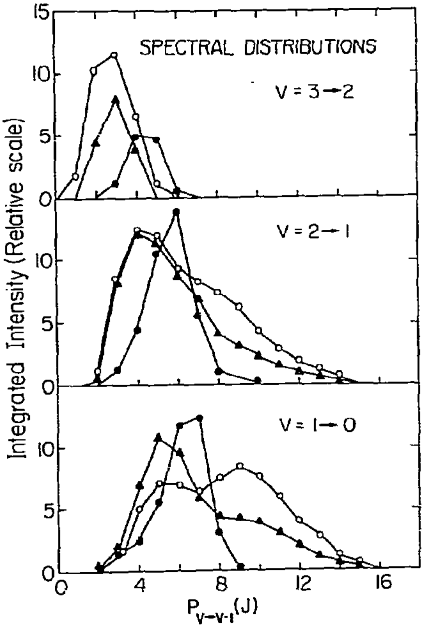

Fig. 9. Spectral distribution of the laser output for the "standard" (●), "P_{Ar} = 0", (▲), and the "no R–T", (○), runs. The intensity scales of the second and third runs are by two and ten times larger than the scale of the standard run, respectively.

the initial distribution in $v = 3$ while the peaks in $v = 2 \rightarrow 1$ and $1 \rightarrow 0$ involve cascading from higher bands.

In the absence of an efficient coupling mechanism between neighbouring radiative transitions, lasing on each line terminates when the effective upper and lower populations are nearly equal. [In the absence of V–T processes, this condition exactly characterizes the final vib-rotational distribution; i.e. $P_f(v,J-1)/(2J-1) = P_f(v-1,J)/(2J+1)$]. Thus, the final vibrational population ratios, $P_f(v)/P_f(v-1)$, are considerably larger than in the fast R–T limit; compare figs. 7a and 7b which correspond to P_{Ar} = 50 and 0 torr, respectively. This behaviour is more pronounced in the "no R–T" case and ideally described in the "no relaxation" case shown in fig. 7c. Since the final distributions corresponding to low R–T rates are still rich in energy (and, as will be shown in the subsequent paper, also in entropy), the laser efficiency is poor compared to that of lasers dominated by fast rotational relaxation.

The effects of the R–T and V–V,T processes on the laser performance are summarized in table 2. The quantities considered in the table have the following meaning: $P_f(v)$ is the vibrational distribution at $t = t_q$, where t_q denotes the quenching time of the laser pulse. The values given for t_q were rounded off because in most runs the laser pulse has a long and low tail. The values of $P_f(v)$ vary slowly in the region $t \approx t_q$. T_f is the temperature of the lasing mixture at $t = t_q$. Since in all runs, except 2,3 and 4, P_{Ar} = 50 torr, the final temperature is very nearly the same, i.e. $T_f \approx 310$ K. The large excess of inert gas prevents considerable temperature rise (the initial temperature is 300 K in all runs). $I(v \rightarrow v-1)/I(v-1 \rightarrow v-2)$ is the ratio between

Table 2
Integrated output characteristics

Run	$P_f(v)$, v=0...3, (%)	$I(1\rightarrow0) : I(2\rightarrow1) : I(3\rightarrow2)$	W/W_{st}	η	η_c	η_p	t_q (μs)	T_f (K)
1 standard	71, 20, 6, 2	1.00 : 1.01 : 0.30	1.00	0.62	0.47	1.62	15	310
2 P_{Ar} = 25 torr	70, 21, 7, 3	1.00 : 1.02 : 0.30	0.98	0.60	0.45	1.55	15	318
3 P_{Ar} = 5 torr	62, 24, 9, 4	1.00 : 1.03 : 0.28	0.91	0.50	0.37	1.28	15	352
4 P_{Ar} = 0	52, 28, 15, 5	1.00 : 1.02 : 0.30	0.76	0.37	0.28	0.97	15	407
5 Boltzmann	72, 20, 6, 2	1.00 : 1.01 : 0.31	0.96	0.66	0.45	1.55	15	310
6 no R–T	37, 33, 23, 7	1.00 : 1.18 : 0.48	0.40	0.25	0.19	0.66	12	310
7 no relaxation	34, 31, 27, 9	1.00 : 1.36 : 0.51	0.64	0.40	0.30	1.04	16	309
8 no V–T	70, 20, 7, 3	1.00 : 1.03 : 0.33	1.20	0.75	0.57	1.97	17	309
9 no V–V	71, 20, 7, 2	1.00 : 0.99 : 0.29	1.00	0.62	0.47	1.62	15	310
10 no V–V, V–T	70, 20, 7, 3	1.00 : 1.02 : 0.32	1.19	0.74	0.56	1.94	17	310
11 no V–T"CF_3"	71, 20, 7, 3	1.00 : 1.06 : 0.32	1.09	0.69	0.52	1.80	17	310

the integrated intensities in bands $v \rightarrow v-1$ and $v-1 \rightarrow v-2$. The total integrated intensity $I = \Sigma I(v \rightarrow v-1)$ is proportional to W, the total laser output energy per unit laser active volume. W/W_{st} measures the total output energy relative to the standard run. We also consider three types of efficiencies, η, η_c and η_p. $\eta \equiv W/E_p$ is the ratio between the total pulse energy to the total amount of *internal* (i.e. vibrotational) energy generated by the pumping reaction. That is, $E_p = N\langle\epsilon_p\rangle$, where $N = [HF]_{t\rightarrow\infty}$ (N in molec/cm^3), and $\langle\epsilon_p\rangle = \Sigma k_2(v,J)E_{vJ}/k_2$ is the average internal energy of a nascent HF molecule. (η is a central quantity in the thermodynamic analyses [2]). $\eta_c = W/E_{av}$ is the chemical efficiency; $E_{av} = N\langle\epsilon\rangle_{av}$, where $\langle\epsilon\rangle_{av}$ is the total (internal + translational) energy of a nascent molecule. Equivalently, $\langle\epsilon\rangle_{av}$ is the exoergicity of the pumping reaction. We have used a common value, $\langle\epsilon\rangle_{av} = 34.55$ kcal/mole for all runs [3], (except for the "Boltzmann" run, no. 5), with $\langle\epsilon_p\rangle = 0.75\langle\epsilon\rangle_{av}$. The proportionality factor is $\langle f_{int}\rangle = \langle f_v\rangle + \langle f_R\rangle = 0.75$. This quantity is the average fraction of the exoergicity of the pumping reaction which appears as product's internal energy. For the nascent vibrotational distribution shown in fig. 3, $\langle f_v\rangle = 0.67$ and $\langle f_R\rangle = 0.08$. In the Boltzmann run $\langle f_R\rangle = \langle\epsilon_R\rangle/\langle\epsilon\rangle_{av} \approx 0.02$. From these considerations it follows that $\eta_c = 0.75\,\eta$ for all runs excluding the Boltzmann run for which $\eta_c = 0.69\,\eta$. Finally, $\eta_p \equiv 3.455\,\eta_c$ represents the average number of photons extracted from an HF molecule. (Assuming an average photon energy of 3500 cm^{-1} = 10 kcal/mole.)

The gradual decrease of the ratios $P_f(v)/P_f(v-1)$ as the rate of R–T increases reflects the efficiency of these processes in converting internal energy into laser light. V–T processes also reduce $P(v)/P(v-1)$ but, of course, compete with rather than support the lasing process. Thus, the highest $P(v)/P(v-1)$ ratios are obtained in the "no relaxation" and "no R–T" runs which also have the poorest efficiencies. The lowest $P(v)/P(v-1)$ ratios and the higest η value are obtained, as expected, for the Boltzmann run. However, the chemical efficiency of the Boltzmann system, η_c, is slightly lower than that of the standard run. This difference implies that rotational relaxation in the standard case (and, if the rotational relaxation model is exact, also in the experiment [3]) is almost, but not absolutely, instantaneous despite the very high inert gas pressure. In fact, we have at least three additional indications which support the conclusion that rotational relaxation, especially of the highly excited J levels, is not perfect. First, as can be seen in fig. 6a, the tails of the rotational distributions in $v = 1$ and $v = 0$ are somewhat overpopulated in comparison with complete Boltzmann populations. Second, the threshold times of the high J levels in the Boltzmann run are somewhat larger than in the standard and the experimental runs. Third, computations of threshold times aiming at simulating the grating selected experiments [3] indicate that the measured threshold times of high J transitions are shorter than those computed by assuming Boltzmann distributions [28]. Of course, the deviation of the standard (and experimental) results from complete rotational equilibrium are minor and should be taken into account only for the calculation of fine details of the laser output spectrum.

The small difference between the chemical efficiencies of the standard and the Boltzmann run can only be attributed to the different degrees of initial rotational excitations and the different rates of rotational relaxation of the high J levels. These highly excited levels are favourably populated by the pumping reaction (in the standard run). Since newly formed HF molecules in high J levels are not immediately relaxed, they contribute to increasing the gain of the high J transitions and thus to the overall laser power.

The inert gas pressure affects the laser efficiency not only through the R–T rates but also through the temperature rise. The temperature rise tends to lower the gain coefficient since it increases both the Doppler and the pressure linewidths. In addition, near rotational equilibrium, the population difference ΔN_{vJ} decreases with T. Yet, for the pressures considered in this study the reduction in the gain coefficient due to the temperature rise is small. In fact, as can be verified from table 2, the reduction in the total laser energy when passing, for example, from run 1 to 4 is less than the reduction in the chemical efficiency. This is due to the fact that in our kinetic model k_2/k_3 increases with T. Consequently, $[HF]_{t\rightarrow\infty}$ increases as P_{Ar} decreases. This effect moderates the reduction of the total pulse energy because of the lower R–T rates. It should be mentioned however that this finding is a direct result of the assumption (which might not be valid) that k_2/k_3 increases with T.

3.3. *Vibrational relaxation*

Vibrational deactivation processes of HF by HF, H, F and H_2 are known to be very fast [1]. However, according to table 2 the reduction in the laser efficiency due to such processes, at least according to the kinetic model employed in this study, is no more than 20%; compare runs 1 and 10. As mentioned in section 3.1, this might be an underestimation of their influence. Nevertheless, more accurate estimates require more reliable kinetic data, especially for the deactivation rates of levels $v \geqslant 2$. Comparison of runs 1 and 11 shows that the arbitrary enhancement of V–T effects by assuming vibrational relaxation due to collisions with free radicals and other possible species does not alter significantly the results.

In addition to lowering the efficiency, V–T processes tend to shorten the laser pulse. In our calculation this effect is pronounced only when the R–T processes are small (compare runs 6 and 7 in table 2 and the pulse shapes in fig. 8). In this case the V–T processes compete only with the direct chemical pumping but not with the (very efficient) indirect pumping by R–T transfer.

Since HF is a highly anharmonic molecule and V–V transfer rates in HF–HF collisions are nearly gas kinetic, Treanor's up-pumping mechanism [29] is very effective in pure HF systems [30,31]. Yet, in the laser system, the V–V processes play a very minor role owing to the presence (in excess) of many other chemical species. The tendency for up-pumping can be observed in table 2 by comparing the results of run 9 with runs 1 and 8.

4. Concluding remarks

We have shown that experimental results can be fairly well reproduced with the aid of a theoretical kinetic model. Further experimental and theoretical information on the various kinetic processes taking place in complex nonequilibrium systems such as the HF chemical laser is still required in order to increase the reliability of modeling studies; not only as analytic but also as predictive tools. The main advantage of these studies is the possibility of testing, eliminating and systematically analyzing the specific effects of different kinetic processes (and optical and mechanical factors) on the behaviour of nonequilibrium systems.

The general guideline of this paper (and the following one [2]) was to study the HF laser as an example of a complex, but relatively well known, nonequilibrium chemical system. Therefore, while treating in detail the radiative, the chemical and the various relaxation processes, we have made several simplifying assumptions concerning other factors. For example, we have assumed that the system is spatially uniform, that the rate equation approximation is valid and that saturation effects, cavity mode structure and off-axial lasing are relatively unimportant. Under some conditions, these assumptions (which are common to most of the modelling studies [5,6,15–20]) may not be justified, e.g. for high power lasers which involve high radiation densities. This however is not the case for the experimental system [3] that served to test our model. Moreover, it should be noted that we have mainly compared relative quantities such as relative intensities of individual lines. These properties are very sensitive to the kinetic parameters of the system but not to the optical-mechanical factors mentioned above.

Acknowledgement

We would like to thank Dr. E. Keren and Professors R.B. Gerber and P. Brumer for their contributions in developing the integration procedure and Mr. D. Brenner for helpfull comments.

Appendix: Numerical values of rate constants

A.1. Initiation

The flash profile shown in fig. 1 was determined by fitting the experimental profile to the expression

$$\psi(t) = A\bar{\psi}(t) = A\,[a_1 t^{n_1} \mathrm{e}^{-b_1 t} + a_2 t^{n_2} \mathrm{e}^{-b_2 t}]\,, \qquad \text{(A.1)}$$

where $\bar{\psi}(t)$ is the normalized profile, $\int \bar{\psi}(t)\,\mathrm{d}t = 1$. The constant A was determined by the requirement [3] that the total reduction in $[CF_3I]$ is $\approx 23\%$. It can be shown that for the conditions employed in the modeling (i.e. $[CF_3I]_0 = [H_2]_0$ and $[CF_3I]_\infty \approx [CF_3I]_0$, $[H_2]_\infty \approx [H_2]_0$) the value of A can be estimated from

$$A \approx [2\alpha/(2-\alpha)]/[1 + k_3/(k_2 + k_3)]\,, \qquad \text{(A.2)}$$

where α is the fractional loss of CF_3I molecules by (R-1) and (R-3). In the standard run we have used $k_3/k_2 = 4.5$ and $A = 0.162$ which yielded $[CF_3I]_\infty/[CF_3I]_0 = 0.75$. The other constants in (A.1) are: $n_1 = 3, n_2 = 13$, $a_1 = 1.019 \times 10^{14}\ s^{-4}, a_2 = 4.564 \times 10^{71}\ s^{-14}\ b_1 = 5.445 \times 10^5\ s^{-1}, b_2 = 2.832 \times 10^6\ s^{-1}$.

The value of k_3 is associated with large uncertainty [21]; $k_3 = (7.5 \pm 3.7) \times 10^{13}\ cm^3$/mole s. We have used $k_3 = 5 \times 10^{13}$ in the standard run; a lower value of k_3 corresponds to higher A and better agreement with the laser experiments.

A.2. Pumping

For k_2 we have used [22], $k_2 = 1.60 \times 10^{14} \times \exp(-800/T)\, cm^3$/mole s. The nascent vibrational distribution is $P(v) = k_2(v)/k_2 = 0, 0.17, 0.56$ and 0.27 for $v = 0,1,2$ and 3, respectively. The rotational distribution is shown in fig. 3.

A.3. Rotational relaxation

The constants in (11) and (12) are: $C = 4.5 \times 10^{-3}$ cm [9] (or 1.5 mole/kcal), $A(T) = (T/300)^{1/2}\ 4.5 \times 10^{13}\ cm^3$/mole s. $\overline{C} = 8.5 \times 10^{-3}$ cm [17], $\overline{A}(T) = (T/300)^{1/2} \times 8.4 \times 10^{12}\ cm^3$/mole s. These values yield, for both models, $k(5\to) = k(5\to4) + k(5\to3) + k(5\to2) \approx 7 \times 10^{13}\ cm^3$/mole s which is close to the estimate in ref. [11] for HF–H_2 collisions. Recall however that (11) or (12) represent the average rate constant for all species.

A.4. Vibrational relaxation

As mentioned in section 2 all V–V and V–T rate constants involving H, F, H_2 and HF were taken from the recommended list of ref. [22].

The values used for k_{12}, (Ar), and k_{13}, (CF_3I), are $k_{12}(v \to v-1) = v(4 \times 10^8)\ cm^3$/mole s [1] and $k_{13}(v \to v-1) = v(8 \times 10^9)\ cm^3$/mole s (estimated by the result for CF_3Br [32]). Deactivation rates for CF_3 and other radicals are not known. In the standard run we used $k_{\text{``}CF_3\text{''}}(v \to v-1) = 0.2, 1, 1 \times 10^{13}\ cm^3$/mole s for $v = 1,2$ and 3, respectively. These values improve somewhat the agreement with the relative band intensities reported in laser experiments and suggest that the relaxation rates of high vibrational levels are underestimated in the kinetic model.

References

[1] N. Cohen and J.F. Bott, in: Handbook of chemical lasers, eds. R.W.F. Gross and J.F. Bott (Wiley, New York, 1976) ch. 2.

[2] A. Ben-Shaul and O. Kafri, Chem. Phys. 36 (1979) 307. (part II of this series), and references therein.

[3] M.J. Berry, J. Chem. Phys. 59 (1973) 6229.

[4] M.J. Berry, in: Molecular energy transfer, eds. R.D. Levine and J. Jortner (Wiley, New York, 1976).

[5] G. Emanuel, in: Handbook of chemical lasers, eds. R.W.F. Gross and J.F. Bott (Wiley, New York, 1976).

[6] K.L. Kompa, Topics in current chemistry, Vol. 37 (Springer, Berlin, 1973).

[7] J.C. Polanyi and K.B. Woodall, J. Chem. Phys. 56 (1972) 1563.

[8] A.M.G. Ding and J.C. Polanyi, Chem. Phys. 10 (1975) 39.

[9] J.C. Polanyi, N. Sathyamurthy and J.L. Schreiber, Chem. Phys. 24 (1977) 105.

[10] N.C. Lang, J.C. Polanyi and J. Wanner, Chem. Phys. 24 (1977) 219.

[11] J.J. Hinchen and R.H. Hobbs, J. Chem. Phys. 65 (1976) 2732;
J.J. Hinchen, Appl. Phys. Letters 27 (1975) 672;
L.H. Sentmann, J. Chem. Phys. 67 (1977) 966.

[12] I. Procaccia and R.D. Levine, J. Chem. Phys. 62 (1975) 2496; 64 (1976) 4570;
R.B. Bernstein, J. Chem. Phys. 62 (1975) 4570;
I. Procaccia, Y. Shimoni and R.D. Levine, J. Chem. Phys. 63 (1975) 3181.

[13] R.D. Levine and A. Ben-Shaul, in: Chemical and biochemical applications of lasers, ed. C.B. Moore (Academic Press, New York, 1977) ch. 4.

[14] R.F. Deutsch, Appl. Phys. Letters 10 (1967) 234; 11 (1967) 18;
H. Pummer and K.L. Kompa, Appl. Phys. Letters 9 (1972) 356;
T.D. Padrick and M.A. Gusinow, Appl. Phys. Letters 22 (1973) 183;
E. Cuellar, J.H. Padrick and G.C. Pimentel, J. Chem. Phys. 61 (1974) 422;
E. Cuellar and G.C. Pimentel, IEEE J. Quant. Electron. QE-11 (1975) 688.

[15] A. Ben-Shaul, G.L. Hofacker and K.L. Kompa, J. Chem. Phys. 59 (1973) 4664, see also U. Schmailzl, A. Ben-Shaul and K.L. Kompa, IEEE, J. Quant. Electron., QE-10, 753 (1974).

[16] A. Ben-Shaul and G.L. Hofacker, in: Handbook of Chemical Lasers, eds. R.W.F. Gross and J.F. Bott (Wiley, New York, 1976) ch. 10.

[17] A. Ben-Shaul, U. Schmailzl and K.L. Kompa, J. Chem. Phys. 65 (1976) 1711.

[18] E. Keren, R.B. Gerber and A. Ben-Shaul, Chem. Phys. 21 (1977) 1.

[19] A. Ben-Shaul, Chem. Phys. 18 (1976) 13.

[20] T.D. Padrick and M.A. Gusinow, Chem. Phys. Letters 24 (1974) 270;
H.L. Chen, R.L. Taylor, J. Wilson, P. Lewis and W. Fyfe, J. Chem. Phys. 61 (1974) 306;
L.H. Sentman, J. Chem. Phys. 62 (1975) 3523;
J.J.T. Hough and R.L. Kerber, Appl. Opt. 14 (1975) 2960;
J.R. Creighton, IEEE, J. Quant. Electron. QE-11 (1975) 699;
R.J. Hall, IEEE, J. Quant. Electron. QE-12 (1976) 453;
G.K. Vasil'ev, E.F. Makarov, A.G. Ryabenko and V.L. Tal'roze, Soviet. Phys. JETP 44 (1976) 690;
L.H. Sentman, Appl. Opt. 15 (1976) 744;
K. Daree and U. Hesse, Opt. Commun. 19 (1976) 269;
M. Baer, Z.M. Top and Z.B. Alfassi, Chem. Phys. 22 (1977) 485.

[21] I.O. Leipunskii, I.I. Morozov and V.L. Tal'roze, Dokl. Akad. Nauk. USSSR 198 (1971) 547;
J. Bozzelli and M. Kaufman, J. Phys. Chem. 77 (1973) 1748.

[22] S.C. Kurzius, Lamp Reaction Models for Analyses of Chemical Lasers, Lockheed Missiles and Space, Comp. Tech. Report RK-CR-75-31 Vol. 3 (1975).

[23] J.C. Polanyi and K.B. Woodall, J. Chem. Phys. 57 (1972);
H.W. Chang and D.W. Setser, J. Chem. Phys. 55 (1973) 2298;
J.G. Moehlmann and J.D. McDonald, J. Chem. Phys. 62 (1975) 3061.

[24] R.D. Meredith and F.G. Smith, J. Quant. Spect. 13 (1973) 89.

[25] D. Proch and J. Wanner, MPI for Plasma Physics (Garching), Report IPP IV/17 (1971).

[26] P. Brumer, J. Comp. Phys. 14 (1974) 391.

[27] C.W. Gear, J. Siam, Num. Anal. 14 (1965) 69.

[28] D. Brenner and A. Ben-Shaul, unpublished results.

[29] C.E. Treanor, J.W. Rich and R.G. Rehun, J. Chem. Phys. 48 (1968) 1798.

[30] H. Pummer, D. Proch, U. Schmailzl and K.L. Kompa, Opt. Commun. 19 (1976) 273.

[31] M. Tabor, R.D. Levine, A. Ben-Shaul and J.I. Steinfeld, Mol. Phys., to be published.

[32] J.F. Bott and N. Cohen, J. Chem. Phys. 61 (1974) 68.